

FIRST RESOLUTION OF MICROLENSED IMAGES*

SUBO DONG,¹ A. MÉRAND,² F. DELPLANCKE-STRÖBELE,² ANDREW GOULD,^{3,4,5} PING CHEN,¹ R. POST,⁶
C. S. KOCHANEK,^{5,7} K. Z. STANEK,^{5,7} G. W. CHRISTIE,⁸ ROBERT MUTEL,⁹ T. NATUSCH,¹⁰ T. W.-S. HOLOIEN,¹¹
J. L. PRIETO,^{12,13} B. J. SHAPPEE,¹⁴ AND TODD A. THOMPSON^{5,7}

¹*Kavli Institute for Astronomy and Astrophysics, Peking University, Yi He Yuan Road 5, Hai Dian District, Beijing 100871, China*

²*European Southern Observatory, Karl-Schwarzschild-Str. 2, 85748 Garching, Germany*

³*Max-Planck-Institute for Astronomy, Königstuhl 17, 69117 Heidelberg, Germany*

⁴*Korea Astronomy and Space Science Institute, Daejeon 305-348, Republic of Korea*

⁵*Department of Astronomy Ohio State University, 140 W. 18th Ave., Columbus, OH 43210, USA*

⁶*Post Observatory, Lexington, MA 02421*

⁷*Center for Cosmology and AstroParticle Physics (CCAPP), The Ohio State University, 191 W. Woodruff Avenue, Columbus, OH 43210, USA.*

⁸*Auckland Observatory, Box 24180, Auckland, New Zealand*

⁹*Department of Physics and Astronomy, University of Iowa*

¹⁰*Institute for Radio Astronomy and Space Research, AUT University, Auckland, New Zealand*

¹¹*The Observatories of the Carnegie Institution for Science, 813 Santa Barbara St., Pasadena, CA 91101, USA 0000-0001-9206-3460*

¹²*Núcleo de Astronomía de la Facultad de Ingeniería y Ciencias, Universidad Diego Portales, Av. Ejército 441, Santiago, Chile*

¹³*Millennium Institute of Astrophysics, Santiago, Chile*

¹⁴*Institute for Astronomy, University of Hawai'i, 2680 Woodlawn Drive, Honolulu, HI 96822, USA*

ABSTRACT

We employ VLTI GRAVITY to resolve, for the first time, the two images generated by a gravitational microlens. The measurements of the image separation $\Delta\theta_{-,+} = 3.78 \pm 0.05$ mas, and hence the Einstein radius $\theta_E = 1.87 \pm 0.03$ mas, are precise. This demonstrates the robustness of the method, provided that the source is bright enough for GRAVITY ($K \lesssim 10.5$) and the image separation is of order or larger than the fringe spacing. When θ_E is combined with a measurement of the “microlens parallax” π_E , the two will together yield the lens mass and lens-source relative parallax and proper motion. Because the source parallax and proper motion are well measured by Gaia, this means that the lens characteristics will be fully determined, whether or not it proves to be luminous. This method can be a powerful probe of dark, isolated objects, which are otherwise quite difficult to identify, much less characterize. Our measurement contradicts Einstein’s (1936) prediction that “the luminous circle [i.e., microlensed image] cannot be distinguished” from a star.

Keywords: gravitational lensing; micro; techniques; interferometric

1. INTRODUCTION

Interferometric resolution of microlensed images is a potentially powerful probe of dark isolated objects (Delplancke et al. 2001). Orbiting dark objects, such as planets, black holes, and old brown dwarfs and neutron stars, can be studied by a variety of techniques, via their impact on their companions. For example, all of these objects can be studied through their gravitational effect on their hosts by radial-velocity and astrometric methods. Planets and brown dwarfs can be studied via their occulting effects using the transit method. Some black holes and neutron stars in binaries can be discovered and characterized because they are accreting gas from stellar companions. Even double-dark objects like black-hole and neutron-star binaries can be detected and studied with gravitational waves.

However, the only known way to study isolated dark objects is with gravitational microlensing. In microlensing, a massive object temporarily magnifies the light of a more distant source in a “microlensing event”. The object can therefore be detected independent of whether it is dark or luminous. The key challenge of microlensing is that the only parameter that can be routinely measured in microlensing events is the Einstein timescale t_E , which is a combination of the lens mass, M , and the lens-source relative (parallax, proper motion), $(\pi_{\text{rel}}, \boldsymbol{\mu}_{\text{rel}})$.

$$t_E = \frac{\theta_E}{\mu_{\text{rel}}}; \quad \theta_E \equiv \sqrt{\kappa M \pi_{\text{rel}}}; \quad \kappa \equiv \frac{4G}{c^2 \text{AU}} \simeq 8.14 \frac{\text{mas}}{M_{\odot}}; \quad (1)$$

where θ_E is called the angular Einstein radius, which is on the order of mas for Galactic microlensing. Hence, for dark microlenses, the only way to recover these three quantities, $(M, \pi_{\text{rel}}, \boldsymbol{\mu}_{\text{rel}})$, separately is to measure θ_E and the “microlens parallax” $\boldsymbol{\pi}_E$ (Refsdal 1966; Gould 1992, 2000, 2004),

$$\boldsymbol{\pi}_E \equiv \frac{\pi_{\text{rel}} \boldsymbol{\mu}_{\text{rel}}}{\theta_E \mu_{\text{rel}}}. \quad (2)$$

By measuring these parameters (θ_E and $\boldsymbol{\pi}_E$), one can then determine

$$M = \frac{\theta_E}{\kappa \pi_E}; \quad \pi_{\text{rel}} = \theta_E \pi_E; \quad \boldsymbol{\mu}_{\text{rel}} = \frac{\theta_E}{t_E} \frac{\boldsymbol{\pi}_E}{\pi_E}. \quad (3)$$

Then, if the source parallax and proper motion ($\pi_s, \boldsymbol{\mu}_s$) can also be measured, one can determine the lens distance and transverse velocity as well.

For dark lenses, there are only three known ways to measure θ_E , and each poses significant challenges. Prior to this paper, the method that had been most successfully applied was to measure the so-called “finite-source effects” as the lens transits the source (Gould 1994a). This yields the microlensing parameter $\rho = \theta_*/\theta_E$,

where θ_* is the angular radius of the source, which can usually be estimated quite well from its color and magnitude (Yoo et al. 2004). The main problem with this method is that the probability that the lens will transit the source for any given microlensing event is equal to ρ , which typically has values $\rho \sim 10^{-2}$ – 10^{-3} .

A second method to measure θ_E is “astrometric microlensing”, wherein one measures the astrometric displacement of the light centroid of the microlensed images from the position of the source. Isolated objects create two images whose offsets from the source and magnifications are given by (Einstein 1936; Paczyński 1986)

$$\boldsymbol{\theta}_{\pm} = u_{\pm} \theta_E \frac{\mathbf{u}}{u}; \quad u_{\pm} \equiv \frac{u \pm \sqrt{u^2 + 4}}{2}, \quad (4)$$

and

$$A_{\pm} = \frac{A \pm 1}{2}; \quad A = \frac{u^2 + 2}{u \sqrt{u^2 + 4}}, \quad (5)$$

where \mathbf{u} is the vector offset of the source from the lens, normalized by θ_E . Hence, the centroid of the light from the images is offset from the position of the source by (Miyamoto & Yoshii 1995; Hog et al. 1995; Walker 1995).

$$\Delta \boldsymbol{\theta}_{i,s} = \left(\frac{A_+ \theta_+ + A_- \theta_-}{A} - u \right) \frac{\mathbf{u}}{u} = \frac{\mathbf{u}}{u^2 + 2} \theta_E. \quad (6)$$

This method of course requires a time series of astrometric measurements because one must simultaneously solve for $(\pi_s, \boldsymbol{\mu}_s)$ in order to determine the intrinsic source position as a function of time, which is a precondition for measuring the “offset” from that position. However, this is also an advantage because, as mentioned above, these quantities are needed to infer the lens distance and transverse velocity once $(\theta_E, \boldsymbol{\pi}_E)$ are measured.

Another advantage of this technique, as discussed by Gould & Yee (2014), is that it actually measures two of the three parameters ($\theta_E, \boldsymbol{\pi}_E$) needed for the mass measurement. That is, it measures both θ_E and the *direction* of $\boldsymbol{\pi}_E$. The reason that this is important is that of the two components of $\boldsymbol{\pi}_E$, the component that is parallel to Earth’s acceleration is much easier to measure than the component that is perpendicular (Gould et al. 1994; Smith et al. 2003; Gould 2004). Hence, if the direction of $\boldsymbol{\pi}_E$ can be independently determined, this dramatically increases the prospects for measuring $\boldsymbol{\pi}_E$ (Ghosh et al. 2004; Gould 2015). While there has been only two reported successful application to date using the *Hubble Space Telescope* (HST) by Sahu et al. (2017) and with HST and VLT/Spectro-Polarimetric High-contrast Exoplanet REsearch (SPHERE) by Zurlo et al. (2018), the prospects for making such measurement with *Gaia* (Gaia Collaboration et al. 2016) are very good as we

discuss below (also see, e.g., [Belokurov & Evans 2002](#); [Bramich 2018](#)).

Here we present the first application of a third method to determine θ_E , interferometric resolution of the microlensed images. As anticipated by [Einstein \(1936\)](#), the mas scale of θ_E for a Galactic microlensing event is far smaller than the resolution of any existing or planned optical telescope for direct resolution of the images. It is, however, possible to do so using interferometry, combining the light from well-separated telescopes to give a much higher angular resolution than the individual elements. Interferometry is routine in radio astronomy and well-developed for small optical telescopes, but has only recently started to become available on large optical telescopes. It is still very challenging and requires a very rare, bright microlensing event. The handful of existing publications on this method ([Delplancke et al. 2001](#); [Dalal & Lane 2003](#); [Rattenbury & Mao 2006](#); [Cassan & Ranc 2016](#)) mainly focus on forecasting its prospects, while here we describe how the actual observational data can be analyzed to constrain microlensing parameters. Like the ‘‘astrometric microlensing’’ method just discussed, it has the important advantage that it can simultaneously measure the direction of $\boldsymbol{\pi}_E$. Stated more succinctly, it can measure $\boldsymbol{\mu}_{\text{rel}}$.

The basic idea of the measurement is straightforward: simply measure the vector separation between the two images, i.e., from the minor image to the major image, $\Delta\boldsymbol{\theta}_{-,+}$. The magnitude of this separation,

$$\Delta\theta_{-,+} = \sqrt{u^2 + 4\theta_E^2} = 2\left(1 + \frac{u^2}{8} \dots\right)\theta_E, \quad (7)$$

directly yields θ_E , given that u is known from the photometric light curve (note that the interferometric data also allow to measure u from the flux ratio between the two lensed images). In fact, as can be seen from the Taylor expansion in Equation (7), for cases that the minor image can be detected with reasonable effort ($u \lesssim 1/2$, see Equation (5)), even very crude knowledge of u is sufficient for an accurate measurement of θ_E .

The direction of $\boldsymbol{\pi}_E$ must be derived from the measurement of $\Delta\boldsymbol{\theta}_{-,+}$ in two steps. In itself, $\Delta\boldsymbol{\theta}_{-,+}$ only gives the direction of the instantaneous separation \mathbf{u} . Then, one must combine this with the angle between \mathbf{u} and $\boldsymbol{\mu}_{\text{rel}}$ to obtain the direction of source motion (or of $\boldsymbol{\pi}_E$). This angle ϕ is given by

$$\phi(u) = \cot^{-1} \frac{(t_{\text{obs}} - t_0)/t_E}{u_0} = \cot^{-1} \frac{\delta t}{t_{\text{eff}}}, \quad (8)$$

and ϕ is always defined to be positive and between 0 and π . Here, (t_0, u_0, t_E) are the [Paczynski \(1986\)](#) parameters describing the trajectory, i.e., $u^2(t) = u_0^2 + (t - t_0)^2/t_E^2$,

t_{obs} is the time of the observation, $\delta t \equiv t_{\text{obs}} - t_0$, and $t_{\text{eff}} = u_0 t_E$ is the effective timescale.

The final form of Equation (8) is very important. In general, t_0 is much better determined than either u_0 or t_E because the latter two are strongly anti-correlated and are also correlated with the source flux f_s and with the blended light f_b that does not participate in the event, via the equation for flux evolution

$$F(t) = f_s A[u(t)] + f_b; \quad u^2(t) = u_0^2 + \frac{(t - t_0)^2}{t_E^2}, \quad (9)$$

and the magnification A is given in Equation (5). Because t_{obs} is known exactly and both t_0 and t_{eff} are usually extremely well-measured, ϕ can be determined very well. Hence, the application of the measurements of both the magnitude and the direction $\Delta\boldsymbol{\theta}_{-,+}$ to the interpretation of the microlensing event depend only very weakly on the precision of the measurement of the lightcurve’s [Paczynski \(1986\)](#) parameters. This feature makes interferometric imaging extremely robust.

Unfortunately, a single epoch of interferometric imaging still leaves an important ambiguity. Because of the way that u_0 enters Equation (9), it is generally the case that only its magnitude is measured, not its sign. In practice, this means that, in the absence of additional information, one does not know whether ϕ should be ‘‘added’’ clockwise or counterclockwise to the direction of $\Delta\boldsymbol{\theta}_{-,+}$ to obtain the direction $-\boldsymbol{\mu}_{\text{rel}}$ (i.e., the source-lens relative proper motion). In fact, this ambiguity can be resolved simply by measuring $\Delta\boldsymbol{\theta}_{-,+}$ at a second epoch. That is, at late times $\mathbf{u} \rightarrow -(t - t_0)\boldsymbol{\mu}_{\text{rel}}/\theta_E$. Hence, ϕ should be ‘‘added’’ to $\Delta\boldsymbol{\theta}_{-,+}$ with the same chirality as the ‘‘motion’’ of $\Delta\boldsymbol{\theta}_{-,+}$ from the first to the second epoch.

In the great majority of cases, it is impossible to tell at the time of the microlensing event whether the lens is dark or luminous simply because the lens is superposed on a relatively bright source. In most cases this determination can be made one or several decades after the event, when the lens and source have separated sufficiently to separately resolve them in high resolution imaging (e.g., [Batista et al. 2015](#); [Bennett et al. 2015](#)). This delay will decrease by a factor of 3–5 with the advent of next-generation (‘‘30 meter’’) telescopes, but it will still be several years. After that wait, the luminous lenses can be further studied but the dark lenses cannot. Therefore, the study of dark isolated lenses requires aggressive observations during the microlensing events, before it is known which lenses are dark.

An interesting class of microlenses whose nature remains to be determined are those giving rise to ‘‘domestic microlensing events’’, i.e., events with sources

within 1–2 kpc of the Sun and lying toward directions other than the $\sim 100 \text{ deg}^2$ that are intensively monitored toward the Galactic bulge. The optical depth for microlensing of these nearby sources is order $\tau \sim 10^{-8}$, i.e., about 100 times lower than toward the Galactic bulge. Moreover, there are only $N \sim$ few million stars in these regions with $V \lesssim 14$, i.e., within the range of amateur observers, who are the only ones who have monitored such large portions of the sky until very recently. Hence, even if these amateurs were 100% efficient, one would expect these events to be detected at only at a rate $\Gamma \sim (2/\pi)N\tau/(t_E A_{\text{min}}) \sim 0.5 \text{ yr}^{-1}/A_{\text{min}}$, where A_{min} is the minimum magnification for detection. These statistics were noted by Gaudi et al. (2008) when the first such $A \approx 40$ event was found by an amateur astronomer A, Tago (Fukui et al. 2007). Of course, with only one such event, nothing definite could be concluded.

Recently, a second such event, TCP J05074264+2447555 (RA=05^h07^m42^s.72, Dec=+24°47′56″.4, Gaia Collaboration et al. 2018; hereafter referred to as “TCP J0507+2447” for brevity), with magnification $A \approx 10$ was found. At this point, the detection of these events still does not strongly contradict theoretical expectations, but reconciliation of theory and experiment does require a somewhat greater efficiency of amateur observers than one might naively expect. Thus, this potential contradiction led our team (as well as many other astronomers, see, e.g., Nucita et al. 2018) to undertake very aggressive observations in order to constrain the nature of this rare event. In our case, we undertook observations with the GRAVITY instrument (GRAVITY Collaboration 2017) of the Very Large Telescope Interferometer (VLTI) to obtain the first measurement of θ_E by interferometric resolution of microlensed images.

2. OBSERVATIONS AND DATA REDUCTION

In this section, we discuss the observations and data reduction of TCP J0507+2447 with a focus on the observing strategy and data reduction of VLTI GRAVITY. The readers who are not familiar with optical interferometry and its terminologies may refer to Lawson (2000) for detailed discussions and Dalal & Lane (2003) for an introduction to interferometry observables in the context of microlensing.

2.1. Observations

The brightening of TCP J0507+2447 was first discovered by the Japanese amateur astronomer Tadashi Kojima (Gunma-ken, Japan) on UT 2017-10-25.688, and the discovery was reported to CBAT “Transient Object Fol-

lowup Reports”¹ on UT 2017-10-31.734. The microlensing nature of the event was recognized using the data from All-Sky Automatic Survey for Supernovae (ASAS-SN; Shappee et al. 2014) made available via ASAS-SN Light Curve Server v1.0 (Kochanek et al. 2017). Jayasinghe et al. (2017) found that the ASAS-SN V -band light curve ending on UT 2017-11-02.41 was consistent with a single-lens microlensing model. Subsequent multi-band imaging follow-up observations were performed at numerous sites. In this work, we use the follow-up data taken with 0.6 m telescopes at Post Observatory (CA and NM, USA) operated by R. Post (RP) in Johnson BV , the 0.5 m Iowa Robotic Telescope (Iowa) at the Winer Observatory (AZ, USA) in AstroDon E-series Tru-balance R and Andover 650FH90-50 longpass filters (which are very similar to Sloan $r'i'$ filters and will be referred to as $r'i'$ throughout the text), the 0.4m telescope of Auckland Observatory (AO) at Auckland (New Zealand) in RI , and the 1.3m SMARTS telescope at CTIO (CT13) in H . The H -band data are calibrated with the Two Micron All Sky Survey (2MASS; Skrutskie et al. 2006), and we add the archival 2MASS H -band measurement of 11.845 ± 0.022 at the baseline to the H -band light curve when modeling the light curve. For all optical and near-infrared (NIR) data, aperture photometry is performed following standard procedures. The light curves are shown in Figure 1. The analysis including more follow-up data, in particular observations with *Spitzer* to obtain space-based microlens parallax constraints (Refsdal 1966; Gould 1994a; Dong et al. 2007), will be reported in a subsequent paper (Zang et al. in prep).

We examined the feasibility of observing this event with the VLTI: the peak limiting magnitude of $K \sim 10$ was observable with the GRAVITY instrument (GRAVITY Collaboration 2017) on the VLTI using the 8-meter Unit Telescopes (UTs). The observation would be at the limit of feasibility due to the low observable altitude of the target ($< 40 \text{ deg}$) and thus its high airmass. Furthermore, the position of the object on the sky also implied that the projection of the baselines on the sky was very much contracted in one direction, giving rise to a lowered spatial resolution in that direction. Despite these limits we decided to submit a Director Discretionary Time (DDT) proposal to the European Southern Observatory. The DDT proposal was accepted on November 6 as DDT 2100.C-5014. The observation was planned for the first possible observation slot available on the UTs, on the nights of November 7 and 8, 2017.

¹ <http://www.cbat.eps.harvard.edu/unconf/followups/J05074264+2447555.html>

The observation was performed by the operational Paranal team led by K. Tristram and X. Hautbois. On the first night, the seeing was excellent. Using the standard mode of GRAVITY (single-feed, visible adaptive optics and fringe tracking on the same star), the fringes could be found easily, but the fringe tracking loop could not be closed continuously. Therefore the observation was a partial success. The data can be used with some limitations explained below. On the second night, the target was fainter and the seeing was worse. The fringes could be briefly seen but could not be tracked, so no useful data were obtained during that night.

2.2. VLTI GRAVITY Data Reduction

We reduced the GRAVITY data using the standard data reduction software (DRS) v1.0.5 (Lapeyrere et al. 2014). The fringe-tracker data were reduced successfully. However, because the observations conditions were far from ideal, we obtained a locking ratio of only $\sim 80\%$, whereas for typical good quality data, this value would be above 99%. The science spectrograph was running with an exposure time of 30 seconds, as a result no frames were recorded with continuous fringe tracking. As a result, all frames from the science spectrograph were rejected because the data reduction software is tuned for the high signal-to-noise (SNR) regime where the fringe tracker is continuously locked. The fringe tracker yields reduced complex visibilities, i.e., amplitude and phase. In principle, both the amplitude and the phase of the visibilities could provide useful information. However, because the data were taken at the end of the night, there were no post-observation calibration observations. This fact, combined with the low locking ratio just mentioned, together implied that the visibility amplitudes could not be used. Hence, our analysis rests entirely on the four 3-telescope closure phases.

The calibrator observed with the microlensing event was BD+15 788, a $K = 8.1$ mag K0III type star, which we selected using the `searchCal`² (Cheli et al. 2016) tool from the Jean-Marie Mariotti Center. The photometric estimate of the angular diameter is 0.12 mas, which means that the object is unresolved for the purpose of our observations. Based on the 90% percentile injected flux in the fringe tracker we estimate that, the overall flux from the microlensing event was 10 times fainter, hence leading to $K \approx 10.6$ mag at the time of observation,

Inspecting the closure phase data shows that the bluest spectral channel is very noisy, which leads to two very different values between our two observation data

sets (which are 10 minutes apart). This is also true for the reddest channel for telescope triangles U4U3U2 and U3U2U1. We subsequently rejected these data points in our analysis. Concerning the error bars given by the DRS, the calibration errors have to be taken into account manually so we added quadratically 0.5 degrees of error, which corresponds to the scatter between our two calibrator data sets.

Ideally, for a four-telescopes configuration, only three closure phases out of four are independent: the fourth being a linear combination of the three others. This is the case if the signal chain is affected only by phase biases per beam (i.e., we ignore closure phase instrumental biases) and if the reduction chain is the symmetrical for all closures. The closure phase redundancy can be broken if the 2-telescopes phases involved in two different closures calculation are not equivalent: for instance, they can be averaged differently when the two closures are averaged. In the case of our data, the combination of four closures has residuals of 1.4 degrees on average, with a scatter of 1.6 degrees RMS. This means that our four closures are not perfectly redundant. We hence chose to fit the four sets of closures, instead of a set of three, since each set of three would result in a different set of parameters.

3. CONSTRAINTS FROM THE PHOTOMETRIC LIGHT CURVES

The photometric light curves of TCP J0507+2447 and the best-fit single-lens model³ are shown in Figure 1. In addition to the 5 parameters (t_0, u_0, t_E, f_s, f_b) of the Paczyński (1986) model, we incorporate the microlens parallax effects, parameterized by $(\pi_{E,E}, \pi_{E,N})$ (Gould 2004) in the fits. We also tried a model with zero blending for all but the ASAS-SN data (ASAS-SN’s resolution is $16''$ and blending from ambient stars cannot be ignored). Blended light is detected at high statistical significance with $\Delta\chi^2 = 182.5$ for 8 additional parameters. The results for both free blending and zero blending models are reported in Table 1.

³ Nucita et al. (2018) reported a short-lived planetary anomaly that they modeled as a companion with planet-to-star mass ratio $q = 1.1 \pm 0.1 \times 10^{-4}$. Our data do not confirm or rule out the planetary deviations from the single-lens model because we did not have the necessary light-curve coverage over the reported anomaly. Nevertheless, we have conducted numerical experiments using the best-fit planetary microlensing models reported in Nucita et al. (2018) and found that the single-lens microlensing parameters relevant to our analysis show negligible changes if we add the reported planetary companion. We also find that the expected magnification and the positions of the major and minor images at the time of the VLTI observations are not affected, and this is because the VLTI data were taken more than 1 week after the reported planetary signals, which occurred at HJD ~ 2458058.5 .

² http://www.jmmc.fr/searchcal_page.htm

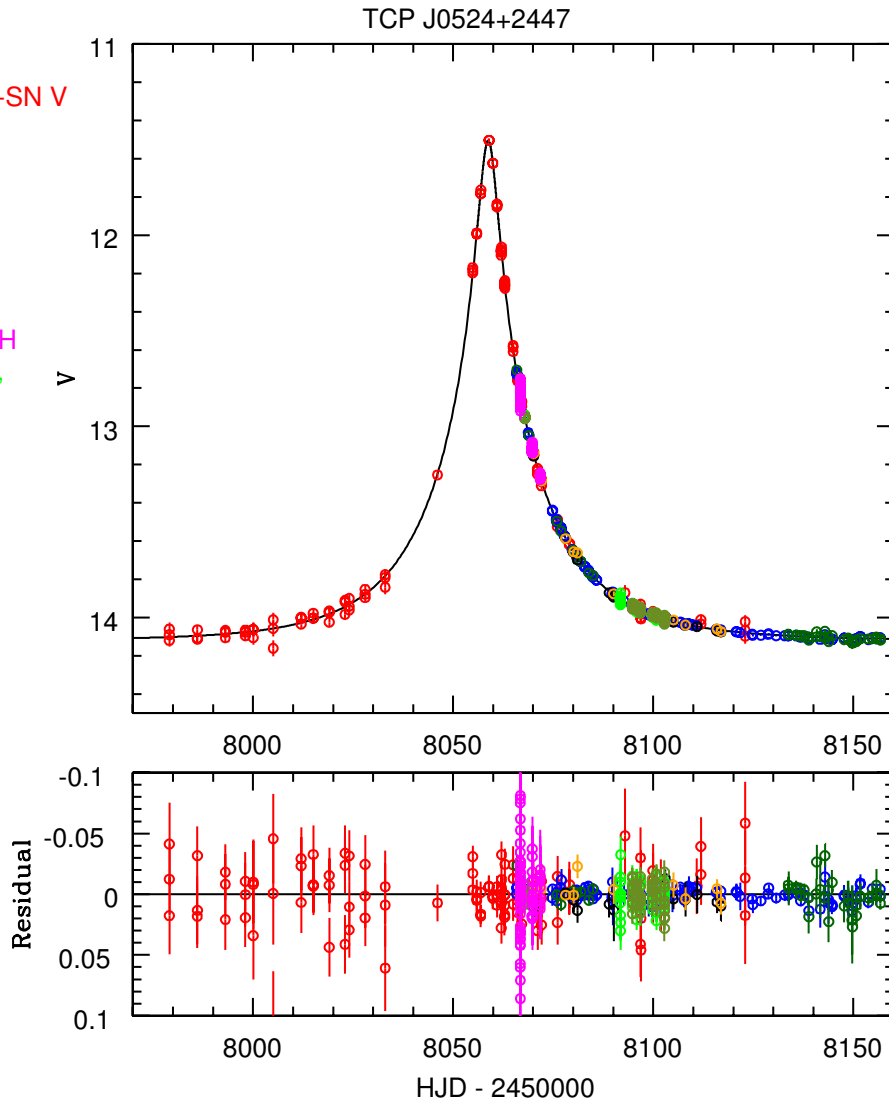


Figure 1. Multi-band light curves of TCP J0507+2447 and the best-fit single-lens model. The data are from ASAS-SN *V*, Post Observatory (RP) in *V* and *B*, Auckland Observatory (AO) *R* and *I*, the 1.3m SMARTS telescope at CTIO (CT13) *H* and the 0.5 m Iowa Robotic Telescope (Iowa) in bands very close to Sloan *r'* and *i'*. All data are photometrically aligned with the *V*-band data using the microlensing model.

The VLTI measurements are made in *K* with a field of view (FOV) of $\sim 0''.05$. The measured blending fraction f_b/f_s from the light curves increases with wavelength. A linear relation between f_b/f_s and the logarithm of the filter central wavelength fits the trend well, and we estimate $f_{b,K}/f_{s,K} = 0.20 \pm 0.02$ for the VLTI bandpass. This implies that the blend is $K \approx 13.6$ based on the 2MASS baseline $K = 11.680 \pm 0.018$. In principle, this blended light could be due to an ambient star within the $\sim 1''$ point spread function (PSF) of the non-ASAS-SN photometric follow-up observations. However, the 2MASS surface density of sources with $K < 13.7$ toward this field is only $\approx 3 \times 10^{-4}$ arcsec $^{-2}$, and the

prior probability of finding an unassociated star within a $1''$ PSF is only $\sim 10^{-3}$. Therefore, the blend is likely associated with the microlensing event: either it is the lens itself, a companion to the lens, a companion to the source or some combination of these possibilities. If the blend were due to the lens, it would lie inside the VLTI FOV. If the blend were a luminous companion to either the lens or the source and within the VLTI FOV, they would face severe restrictions from the microlensing light curves in the form of binary-lens perturbation or binary-source signals. The companion might instead be distant enough to be outside the VLTI FOV and unconstrained from the light curve modeling. We defer the detailed dis-

Parameters	Free blending	Zero blending
t_0 (HJD)-2450000	8058.76 ± 0.01	8058.74 ± 0.01
u_0	0.084 ± 0.001	0.089 ± 0.001
t_E (days)	27.92 ± 0.38	26.46 ± 0.08
$\pi_{E,E}$	0.05 ± 0.15	0.56 ± 0.07
$\pi_{E,N}$	0.20 ± 0.84	0.19 ± 0.42
$f_{b,B}/f_{s,B}$	0.043 ± 0.017	0
$f_{b,V}/f_{s,V}$	0.063 ± 0.017	0
$f_{b,r'}/f_{s,r'}$	0.083 ± 0.017	0
$f_{b,R}/f_{s,R}$	0.105 ± 0.018	0
$f_{b,i'}/f_{s,i'}$	0.112 ± 0.018	0
$f_{b,I}/f_{s,I}$	0.141 ± 0.019	0
$f_{b,H}/f_{s,H}$	0.182 ± 0.018	0
A_{VLTI}	3.87 ± 0.05	3.687 ± 0.004
u_{VLTI}	0.266 ± 0.003	0.2791 ± 0.0003
χ^2	542.6	725.1

Table 1. Best-fit parameters and uncertainties for single-lens models with free blending parameters and fixed zero blending parameters. The predicted magnifications at the time of VLTI observations (HJD_{VLTI} = 2458065.8) A_{VLTI} and u_{VLTI} are also reported. In total, there are 539 data points, and the best-fit χ^2 values for both model are reported too.

cussion on the light-curve constraints on the companion to a follow-up paper (Zang et al. in prep). In the following section, we model the VLTI data by assuming both possibilities. The magnification at the time of VLTI observations is well constrained to be $A_{\text{VLTI}} = 3.87 \pm 0.05$ (i.e., $u_{\text{VLTI}} = 0.266 \pm 0.003$).

4. MODELING THE INTERFEROMETRIC DATA

Because this is a microlensing event, there are guaranteed to be at least three effectively point sources in the field, i.e., the lens and the two images of the source. As discussed above, the blend detected from light-curve modeling can be due to the lens or luminous companions to the lens and/or source outside the VLTI FOV. We have limited ability to directly address these with the interferometric data. Hence, we proceed to analyze the VLTI data using two sets of models: 1) assuming that there is negligible light from the lens (“no lens light”) and 2) assuming that the blend is the lens (“luminous lens”).

4.1. Simplest Model: No Lens Light

In our first analysis, we assume that there is no light from the lens, so that the FOV of VLTI contains only

a “binary star”, formed by the two lensed images. We treated these images as unresolved by the interferometer. We apply the well-verified CANDID software⁴ (Galenne et al. 2015) to model the closure phases and find

$$\begin{aligned} \Delta\theta_{-,+} &= 3.75 \pm 0.03 \text{ mas}, & \psi &= -5.5^\circ \pm 0.3^\circ; \\ \eta &= 0.546 \pm 0.032, \end{aligned} \quad (10)$$

where $\Delta\theta_{-,+}$ is the scalar separation, ψ is the position angle (North through East), and η is the flux ratio. The χ^2 of the fit is 25.5. Since we have two data sets, each with 14 data points, and three fitted parameters, the number of degrees of freedom is 25, yielding a reduced χ^2 of 0.98. Figure 2 shows the closure phase data and the best-fit model (left), and the 4-telescope (4T) configuration at the time of observations. The visibility and phase function for the best model in the u, v plane are shown in the lower right panel of Figure 2.

Without referencing the microlensing light curves, we can estimate the magnification, $A = (1 + \eta)/(1 - \eta) = 3.38 \pm 0.21$. Inverting Equation (5), this yields

$$u = \sqrt{2/\sqrt{1 - A^{-2}} - 2} = 0.306 \pm 0.022 \quad (11)$$

Hence,

$$\theta_E = \frac{1}{\sqrt{1 + u^2/4}} \frac{\Delta\theta_{-,+}}{2} = 1.850 \pm 0.014 \text{ mas} \quad (12)$$

Note in particular that the fractional uncertainty in the first factor in Equation (12) is only 0.16%. Hence, the error in the estimate of θ_E is completely dominated by the error in $\Delta\theta_{-,+}$. The model of the apparent image is illustrated in the upper right panel of Figure 2.

The derived $u = 0.305 \pm 0.020$ is in 2σ tension with the value estimated from light-curve modeling $u_{\text{VLTI}} = 0.266 \pm 0.003$. We also attempt to impose the prior $u = 0.266 \pm 0.003$ to the CANDID models. The best-fit model has a only marginal increase of $\Delta\chi^2 = 1.75$, and the best-fit values $\theta_E = 1.837 \pm 0.012 \text{ mas}$ and $\psi = -5.14^\circ \pm 0.29^\circ$ are within 1σ of those given in Equations (10) and (12). Therefore, the VLTI data have much weaker constraint on u /magnification, and imposing the magnification prior from the photometric models hardly change the derived θ_E and ψ .

CANDID allows free searches for “third body companions” to binary stars. We conducted such a search but did not find any statistically significant local minima. Of course, this does not rule out the presence of other sources: it only means that we cannot probe for other

⁴ <https://github.com/amerand/CANDID>

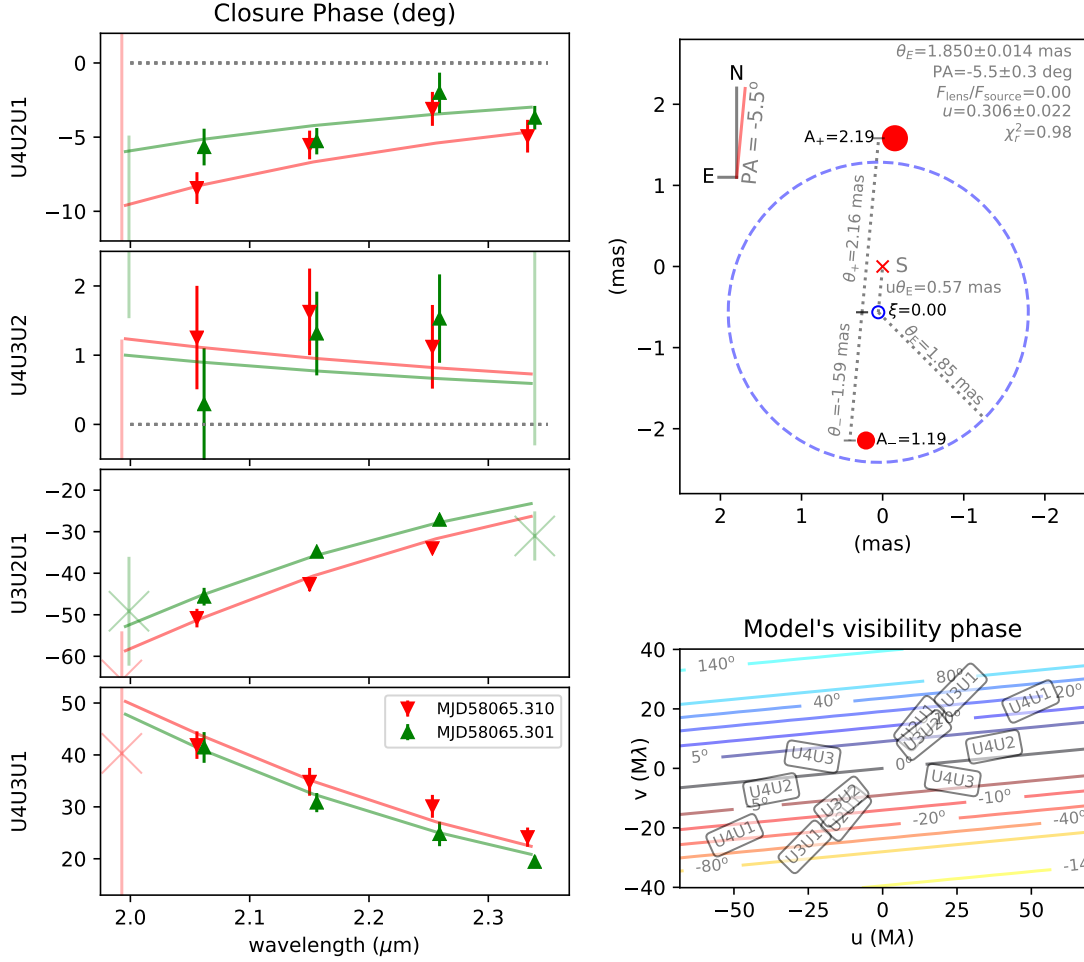


Figure 2. VLTI model with no lens light. Left: closure phase data (points and error bars) and model (continuous lines) for the four sets of telescope triangles, as function of wavelength. The 2 data sets, represented by 2 different symbols, have been slightly offset in wavelength for clarity. Upper Right: model of the apparent images. The two red dots are the major and minor images (note that the size of the dots does not represent the actual apparent sizes of the images), the 'x' symbol in red is the un-lensed source position (labeled "S"). The lens position is shown as a blue open circle, and the dashed circle is the Einstein ring. The flux of each component (minor/major images, lens) is given in fractions of un-lensed source flux. Lower Right: visibility and phase function for the best model in the u, v plane, as well as our 4T configurations at the time of observations. The colored lines are contour lines showing the visibility phase (in degrees), blue for positive phase and red for negative phase, indicating the orientation of the "binary".

sources without specifying their positions. The other potential source for which we actually know the position is the lens. So we next analyze the data within the context of such "restricted 3-body" models.

4.2. Models With a Luminous Lens

To conduct such modeling, we re-parameterize the problem so that the lens will automatically be positioned correctly relative to the two images of the source. We use parameters (θ_E, ψ, u, ξ) , where $\xi = f_l/f_s$ and f_l is the flux from the lens and f_s is the flux of the source, un-amplified. Then, from Equation (5), we infer A_{\pm} , and from Equation (4), we infer θ_{\pm} , i.e., separations

from the lens (which is at origin) along opposite directions specified by ψ . The ratio of the "secondary" (minor-image) to the "primary" (major-image) flux is then $\eta = (A - 1)/(A + 1)$, while the ratio of lens flux to the "primary" is $2\xi/(A + 1)$.

We impose the priors that $u = u_{VLTI} = 0.266 \pm 0.003$ and $\xi = f_{b,K}/f_{s,K} = 0.20 \pm 0.02$ based on the best-fit photometric models. The best-fit model, as illustrated in Figure 3, has a reduced χ^2 of 1.20, which is $\Delta\chi^2 = 5.5$ worse than the "no lens light" VLTI model with no external prior. The best-fit parameters are,

$$\theta_E = 1.891 \pm 0.014 \text{ mas}; \quad \psi = -4.9^\circ \pm 0.3^\circ. \quad (13)$$

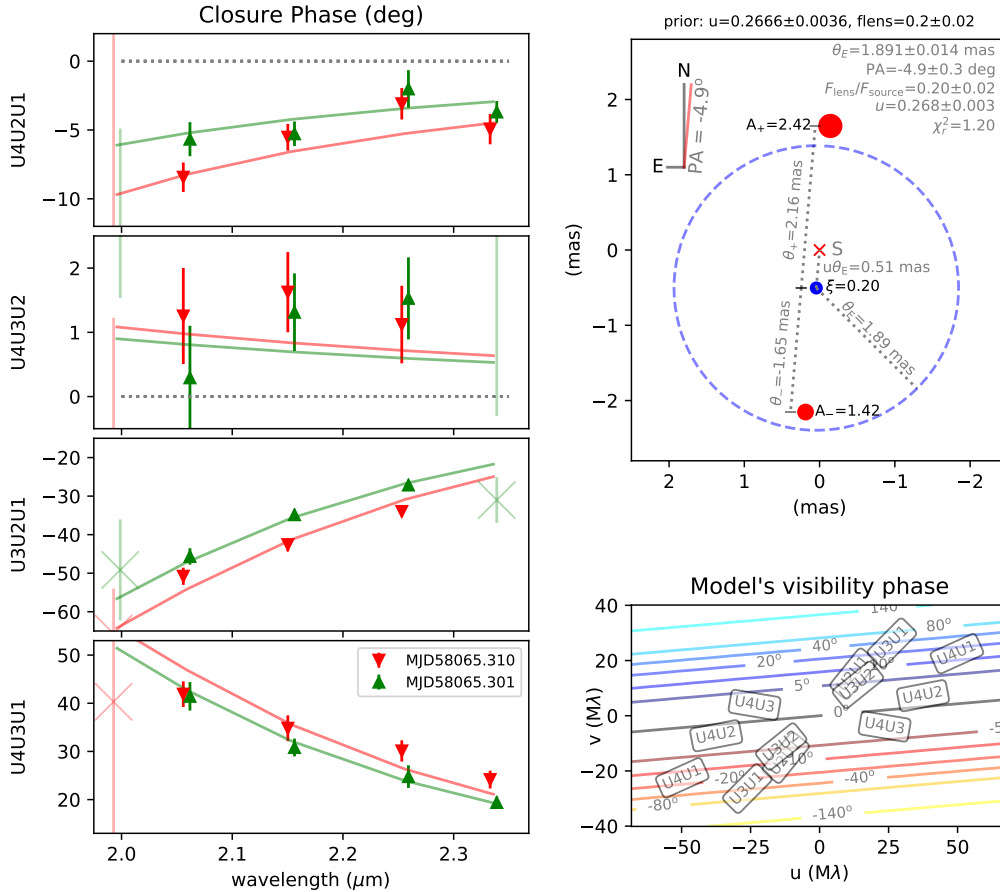


Figure 3. The VLTI model with a luminous lens. The panels are the same as in Figure 2.

These values are only $\approx 2\sigma$ different from the values in Equations (12) and (10) of the “no lens light” VLTI model.

Therefore, the present VLTI data only weakly constrain the magnification and lens flux. The interferometric angular Einstein radius is robustly estimated to the 1–2% level, independent of whether or not the lens contributes to the flux detected in the VLTI FOV.

Finally, we determine ϕ , the angle between the instantaneous source-lens separation, u , and the direction of source-lens relative proper motion, $-\mu_{\text{rel}}$. Recall that this quantity depends only on the photometric light curves, via the parameters t_0 and t_{eff} . We find $(t_0, t_{\text{eff}}) = (8058.76, 2.35) \pm (0.01, 0.02)$, and these yield,

$$\phi = \cot^{-1} \frac{\delta t}{t_{\text{eff}}} = 18.4^\circ \pm 0.2^\circ. \quad (14)$$

As discussed in Section 1, because we have interferometric data at only a single epoch, we cannot determine whether ϕ should be added or subtracted from ψ to find the direction of relative source-lens motion. That is, this direction could be either $12.9^\circ \pm 0.4^\circ$ or

$-23.9^\circ \pm 0.4^\circ$ (North through East) based on the “no lens light” model; and either $13.5^\circ \pm 0.4^\circ$ or $-23.3^\circ \pm 0.4^\circ$ (North through East) for the “luminous lens” model. As discussed in Section 1, the direction of the microlens parallax π_E is defined as that of lens-source proper motion, and thus its direction $\Phi_\pi^{u_0^+} = \pi + \theta - \psi$ (for the positive u_0 solution) or $\Phi_\pi^{u_0^-} = \pi + \theta + \psi$ (for the negative u_0 solution). The relevant geometry is shown in Fig. 4. We discuss in Section 5.2 how this ambiguity can ultimately be resolved using *Gaia* and/or *Spitzer* data.

5. DISCUSSION

In summary, using VLTI GRAVITY, we successfully resolve the images of a microlensing event for the first time. As a result, we obtain a precise measurement of the angular Einstein radius regardless of whether or not a luminous lens contributes to the flux detected in the VLTI FOV: $\theta_E = 1.850 \pm 0.014 \text{ mas}$ for the “no lens light” model and $\theta_E = 1.883 \pm 0.014 \text{ mas}$ for the “luminous lens” model.

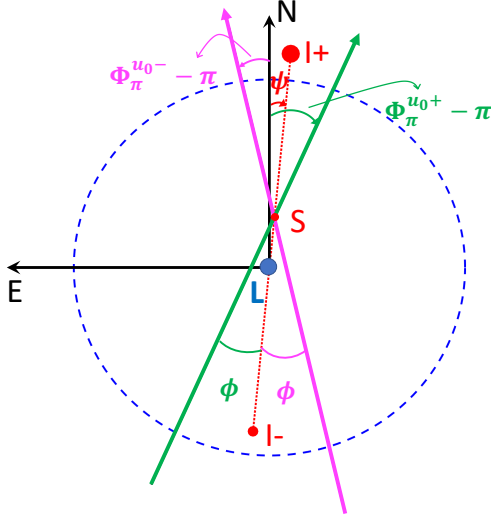


Figure 4. The geometry of the microlensing model. North is up and East is to the left. The lens (“L”) position is shown as a blue dot, and the Einstein ring is represented by a circle in blue dashed line. The source position at the VLTI measurement is shown as a red dot labelled with “S”, and the two images are shown as two red dots labelled with “I+” (major) and “I-” (minor). The position angle of the two images from North through East is defined as ψ , and this is a VLTI observable. There are two degenerate solutions of the lens-source trajectory angle Φ_π measured from North through East, and the two trajectories are shown in blue and magenta lines, respectively, with the arrows indicating the direction of the source-lens relative proper motion. The angle ϕ between the source-lens relative proper motion and source-lens relative position can be determined directly from the light-curve parameters (see Eq. 8). The two degenerate solutions are $\Phi_\pi^{u_0^+} = \psi - \phi + \pi$ and $\Phi_\pi^{u_0^-} = \psi + \phi + \pi$ for positive and negative u_0 , respectively. Note that, in this plot, an angle with a clockwise arrow has a negative value, and the angle ϕ is always positive by definition.

5.1. Comparison with the Nucita et al. (2018) θ_E measurement

Nucita et al. (2018) reported a short-duration planetary anomaly near the peak of their TCP J0507+2447 light curves, and by modeling the finite-source effects when the source passed by the planetary caustics, they measured $\rho \equiv \theta_*/\theta_E = (6.0 \pm 0.8) \times 10^{-3}$, where θ_* is the angular size of the source. Nucita et al. (2018) made a rough estimate of θ_* by assuming that the source distance is in the range of 700-800 pc. In what follows, we use the tight empirical color/surface-brightness relation of Kervella et al. (2004) to estimate θ_* , which is a commonly adopted approach in microlensing works (Yoo et al. 2004).

To estimate the source radius θ_* , we first evaluate the apparent magnitude of the source in two bands, V_s and

K_s . For the former, we simply adopt the value from the fit to the microlensing event, $V_s = 14.207$. For the latter, we first note the 2MASS baseline value $K_{\text{base}} = 11.68$ and then take account of the $f_{b,K}/f_{s,K} = 0.20$ blending in K -band to derive $K_s = 11.88$. Hence, the observed color is $(V - K)_s = 2.327$. Next we note that the CMB extinction toward this direction is $A_{V,\text{CMB}} = 1.579$ and $A_{K,\text{CMB}} = 0.174$ (Schlafly & Finkbeiner 2011), implying $E(V - K)_{\text{CMB}} = 1.405$. The source has been spectroscopically typed as F5V (Maehara et al. 2017), for which $(V - K)_{s,0} = 1.08$ (Pecaut & Mamajek 2013). We infer that the source lies behind a fraction $\lambda = [(V - K)_s - (V - K)_{s,0}]/E(V - K)_{\text{CMB}} = 0.89$ of the CMB extinction. The source ($l=178.756$, $b=-9.325$) is about 125 pc above the plane by using $\pi_{\text{Gaia}} = 1.45$ mas, and given that the dust scale height is about 100 pc and also that the dust density declines toward the direction of the source (i.e., in the anti-center direction), this value of λ is in the expected range. Hence, we find that the de-reddened source fluxes are $V_{s,0} = 12.80$ and $K_{s,0} = 11.72$. Using the color/surface-brightness relation of Kervella et al. (2004), we obtain $\theta_* = 9.0 \mu\text{as}$, and the overall error on this procedure is about 10%. We note that if we simply use the values $R_{*,\text{Gaia}} = 1.49 R_\odot$ and $\pi_{\text{Gaia}} = 1.45$ mas based on Gaia DR 2, then we obtain $\theta_* = 10.0 \mu\text{as}$. However, given that the Gaia “star” is actually a blend of the source and a closer and redder blend, this result is consistent with the estimate based on the color/surface-brightness relation.

We then combine this result with the measurement by Nucita et al. (2018) of $\rho \equiv \theta_*/\theta_E = (6.0 \pm 0.8) \times 10^{-3}$, to obtain $\theta_E = 1.50 \pm 0.25$ mas. This compares to the much more precisely derived value of $\theta_E = 1.87 \pm 0.03$ mas (considering both the “no lens light” and “luminous lens” solutions) in the present work. Therefore, we find that the two agree at the 1.5σ level. This agreement gives added confidence to the planetary interpretation of the anomaly found by Nucita et al. (2018).

5.2. Future mass, distance, and transverse velocity measurements

Recall from Equation (3) that by measuring θ_E and π_E , one can immediately determine $(M, \pi_{\text{rel}}, \mu_{\text{rel}})$. Since the source star is bright, the Gaia second data release (DR2) already has a very accurate measurement of π_s and μ_s : $\pi_{\text{Gaia}} = 1.451 \pm 0.031$ mas and $(\mu_{\text{RA,Gaia}} = -0.229 \pm 0.061$ mas/yr, $\mu_{\text{Dec,Gaia}} = -7.33 \pm 0.033$ mas/yr).⁵ Hence, this would immediately yield

⁵ More precisely, what Gaia actually measures is the flux-weighted mean parallax and proper motion of all sources within the Gaia point spread function (PSF), $\text{FWHM}_{\text{Gaia}} \sim 100$ mas.

the lens distance $D_l = \text{AU}/(\pi_{\text{rel}} + \pi_s)$ and transverse velocity $\mathbf{v}_\perp = D_L(\boldsymbol{\mu}_{\text{rel}} + \boldsymbol{\mu}_s)$. Because GRAVITY has already measured θ_E , the only missing ingredient is $\boldsymbol{\pi}_E$.

As briefly mentioned in Section 1, it is generally substantially easier to measure $\boldsymbol{\pi}_E$ if its direction Φ_π is known independently. As we discuss below, this will be case for TCP J0507+2447. As also mentioned in Section 1, two epochs of interferometric imaging yield this direction, but a single epoch determines the direction only up to a two-fold ambiguity, $\Phi_\pi = \pi + (\psi \pm \phi)$. As illustrated in Fig. 4, here ψ is the position angle of the major image with respect to the minor image and ϕ is the angle between the source-lens separation vector and the direction of source-lens relative motion.

Unfortunately, as noted in Section 2, interferometric data could only be obtained over an interval of a few minutes. Hence this ambiguity in Φ_π remains.

5.2.1. Resolution of the Direction Ambiguity with Gaia

To understand how *Gaia* can resolve the directional ambiguity, we begin by considering a series of N astrometric measurements carried out uniformly over time T , each with error σ_0 in each direction, and with the conditions $T/N \ll 9t_E \ll T$. (We explain the reason for the “9” further below). Because $N \gg 1$, the parallax and proper motion of the source will be measured with much higher precision than the individual measurements, and indeed because $9t_E \ll T$, they will be measured much better than any astrometric quantity that can be derived from measurements during $\mathcal{O}(9t_E)$. Hence, for our purposes, we can regard the true position of the source as “known perfectly”. The error in the measurement of the offset of the image centroid from the source is then simply the error in the former. Hence, we can write the SNR of the ensemble of measurements of these offsets as

$$\begin{aligned} (\text{SNR})^2 &= \sum_{i=1}^N \frac{u_i^2 \theta_E^2}{(u_i^2 + 2)^2 \sigma_0^2} \\ &= \sum_{i=1}^N \frac{(u_0^2 + (t_i - t_0)^2/t_E^2) \theta_E^2}{(u_0^2 + (t_i - t_0)^2/t_E^2 + 2)^2 \sigma_0^2}. \end{aligned} \quad (15)$$

Because $\theta_E \ll \text{FWHM}_{\text{Gaia}}$, this implies that the *Gaia* parallaxes and proper motions will always be weighted means of the source and lens flux: $\pi_{\text{Gaia}} = (\pi_s + r_{\text{Gaia}} \pi_l)/(1 + r_{\text{Gaia}})$, where $r_{\text{Gaia}} = f_{l,\text{Gaia}}/f_{s,\text{Gaia}}$, and similarly for $\boldsymbol{\mu}_{\text{Gaia}}$. Note that if (as in the present case) $r_{\text{Gaia}} \ll 1$, then $\pi_{\text{Gaia}} \simeq \pi_s + r_{\text{Gaia}} \pi_{\text{rel}}$. If we now identify $f_l = f_b$, then using Table 1, we obtain $r_{\text{Gaia}} \simeq (r_V + r_B)/2 \simeq 0.053$. This implies that the fractional correction to the naive *Gaia* parallax is $\simeq 5.3\%(\pi_{\text{rel}}/\pi_s)$, which is likely to be of order or somewhat larger than the *Gaia* statistical error. Therefore, this correction must be taken into account once $\pi_{\text{rel}} = \pi_E \theta_E$ is measured.

In most cases of interest (including the present one), $u_0^2 \ll 2$. Hence we can approximate $u_0 \rightarrow 0$. Making use $T/N \ll 9t_E$, we can approximate the sum as an integral, and then making use of $9t_E \ll T$ we can take the limits of this integral to infinity,

$$\begin{aligned} (\text{SNR})^2 &\rightarrow \frac{\theta_E^2 N t_E}{\sigma_0^2 T} \int_{(-T/2-t_0)/t_E}^{(T/2-t_0)/t_E} d\tau \frac{\tau^2}{(\tau^2 + 2)^2} \\ &\simeq \frac{\theta_E^2 N t_E}{\sigma_0^2 T} \int_{-\infty}^{\infty} d\tau \frac{\tau^2}{(\tau^2 + 2)^2}, \end{aligned} \quad (16)$$

where $\tau \equiv (t - t_0)/t_E$. This is easily evaluated

$$\text{SNR} \rightarrow \frac{\theta_E}{\sigma_{\text{tot}}} \sqrt{\frac{t_E}{T} \frac{\pi}{8^{1/2}}} \simeq \frac{\theta_E}{\sigma_{\text{tot}}} \sqrt{\frac{t_E}{T}} \quad (17)$$

where $\sigma_{\text{tot}} \equiv \sigma_0/\sqrt{N}$ is the astrometric precision of the position measurement from the entire series of observations. From Equation (16) we see that the maximum value of the integrand is 1/8, while from Equation (17) we see that the value of the integral is $(\pi/8^{1/2})t_E$. Hence the effective width of the integral is the ratio of these, i.e., $t_{\text{width}} = 8^{1/2}\pi t_E \simeq 9t_E$. This is the reason that the quantity defining the extreme limits is “ $9t_E$ ” rather than simply “ t_E ”.

The fractional error in the θ_E measurement as well as the angular error (in radians) of Φ_π are both equal to $(\text{SNR})^{-1}$.

For *Gaia* measurements of TCP J0507+2447, the condition $u_0^2 \ll 2$ is well satisfied. To evaluate the conditions, $T/N \ll 9t_E \ll T$, we first note that $9t_E \sim 0.7$ yr, compared to $T = 5$ yr for the baseline *Gaia* mission. Hence, $9t_E \ll T$ is reasonably satisfied. Second, for targets near the ecliptic, *Gaia* can be expected to make about 35 visits (each composed of two observations) over 5 years, which are restricted to $\sim 70\%$ of the year by the Sun exclusion angle. Hence $(T/N)_{\text{eff}} \sim 0.1$ yr. Hence, $T/N \ll 9t_{\text{eff}}$ is also reasonably satisfied.

If we adopt a 5-year mission precision of *Gaia* for a $V = 14$ source of $\sigma_{\text{tot}} \sim 25 \mu\text{as}$, then we obtain

$$\sigma(\Phi_\pi) \simeq \frac{25 \mu\text{as}}{1.8 \text{ mas}} \sqrt{\frac{27 \text{ day}}{5 \text{ yr}} \frac{57^\circ}{\text{rad}}} = 6.6^\circ. \quad (18)$$

This error bar should be compared to the difference in the angles between the two solutions $2\phi = 37^\circ$. Hence, it is very likely that *Gaia* can resolve the ambiguity in Φ_π . Recall that because of the much higher precision of the GRAVITY measurement of ψ , the role of *Gaia* is only to break the ambiguity, not actually measure Φ_π .

For completeness, we note the following facts about uniform astrometric monitoring of microlensing events, even though they are not directly relevant to the case

of TCP J0507+2447. First, if one were to take account of improved astrometry of magnified images (due to the fact that they are brighter), this would lead to a modification of Equation (17). If (as in the case of TCP J0507+2447), the astrometric errors are decreased by a factor $A^{-1/2}$, then one easily finds that the continuous formula changes by $\pi/2^{3/2} \rightarrow 2^{1/2} \ln(2^{1/2} + 1)$. On the other hand, for much fainter (“below sky”) targets for which the errors are reduced by A^{-1} , we have $\pi/2^{3/2} \rightarrow \pi/2$. The main importance of these formulae is that they are not very different, i.e., they lead to improvements of SNR by factors 1.12 and 1.19, respectively. However, the main reason for not using the first formulae here is that its conditions for use are $[(T/N \ll t_E) \& (9t_E \ll T)]$ (rather than $T/N \ll 9t_E \ll T$). This condition is not met by *Gaia* for TCP J0507+2447 and indeed will never be met for any *Gaia* event because it implicitly requires $N \gg 9^2$. However, the second (“below sky”) formula only requires $T/N \ll t_E \ll T$ and so might plausibly be met by some faint, *Gaia*-microlensing black-hole candidates.

Finally, we note that Equation (17) can easily be generalized to the case of $u_0 \neq 0$ by $\pi/2^{3/2} \rightarrow \pi(1+u_0^2)/(2+u_0^2)^{3/2}$. It is of some interest to note that this formula peaks at $u_0 = 1$ and that it only falls back to $\pi/2^{3/2}$ at $u_0^2 = (1 + \sqrt{5})/2$. This means that astrometric events can be detected and well measured even when there is no obvious photometric event. The “below sky” formula is also easily generalized: $\pi/2 \rightarrow \pi/\sqrt{4+u_0^2}$. Unfortunately, the generalization of the “above sky” formula can not be written in closed form.

5.2.2. Future Parallax Measurement

Unfortunately, the photometric light curves do not yield useful parallax information. The event is quite short compared to a year, so only if π_E were extremely large would we expect a full measurement of π_E from the annual-parallax effect. Nevertheless, one might have hoped to measure the component parallel to Earth’s acceleration, $\pi_{E,\parallel}$, which would induce an asymmetry in the light curve.

However, the event lies quite close to the ecliptic and it peaked only three weeks from opposition. Hence, the component of Earth’s acceleration transverse to the line of sight is only 1/3 of its full amplitude. In addition, by chance the lens-source relative proper motion points roughly south whereas Earth’s acceleration points roughly east. Combined, these factors imply that the light-curve asymmetry induced by Earth’s acceleration is only about 1/10 of what it could be for the most favorable geometry. Thus, it is not surprising that there is no detectable signal.

Fortunately, *Spitzer* has taken a series of observations covering its visibility window, $1.7 < (t - t_{0,\oplus})/t_E < 3.1$. As we now argue, it will probably not be possible to properly interpret these observations until Φ_π is determined by combining *Gaia* data with our interferometric measurement (as described in Section 5.2.1). Hence, we present here the general principles of such a measurement, which would be the first from such late-time *Spitzer* observations, and we explain how these rest critically on the precision of the measurement that we have made of ψ .

In general, space-based parallax measurements derive from a time series of space-based photometric measurements. If these measurements cover the peak and wings of the event as seen from space, then one can directly measure $t_{0,\text{sat}}$ and $u_{0,\text{sat}}$ from the light curve. Then by comparing these to $t_{0,\oplus}$ and $u_{0,\oplus}$ measured from the ground (and knowing the projected separation of the satellite from Earth, \mathbf{D}_\perp), one can determine π_E (Refsdal 1966; Gould 1994a). If (as is very often the case for *Spitzer* observations), only the post-peak tail of the light curve is observed from space, then it is impossible to measure $t_{0,\text{sat}}$ and $u_{0,\text{sat}}$ from the satellite light curve alone. However, using color-color relations linking the ground-based and space-based data, one can determine the space-based source flux independent of the space-based light curve. With this added information, it is possible to extract the full π_E from even a post-peak light curve (Calchi Novati et al. 2015).

However, the case of TCP J0507+2447 is substantially more extreme than any previous one. We know that at the first observation $\tau \equiv (t - t_{0,\oplus})/t_E = 1.7$. Moreover, although we do not know the precise angle of $\Phi_\pi = \pi + (\psi \pm \phi)$, we do know that it is roughly due south, whereas *Spitzer* lies roughly to the west. Hence, the Einstein-ring distances τ and $\pi_E D_\perp/\text{AU}$ add approximately in quadrature. So, for example, if $\pi_E = 1$, then (with $D_\perp \sim 1.4 \text{ AU}$), $u_{\text{sat}} \sim 2.2$ at the first observation. This would imply $A = 1.045$. While such a small magnification is likely measurable for the bright source in this event, it is less clear that (t_0, u_0) could be reconstructed from a falling light curve starting at such a low level.

Fortunately, this is not actually necessary. Because we know (or, after the *Gaia* measurement, will know) Φ_π very well, and we know the direction of *Spitzer* extremely well, we will also know the angle between them. This will then permit us to employ a variant of the idea proposed by Gould & Yee (2012) (and verified by Shin et al. 2018) of “cheap space-based parallaxes”. They showed that with just one or two space-based photometric measurements taken near $t_{0,\oplus}$ (plus a late-time

“baseline” measurement) one could measure π_E for high-magnification ($u_0 \ll 1$) events.

We now show that the same is true even if the measurements are taken well after peak, *provided* that one knows Φ_π independently. Let γ be the (known) angle between the satellite and π_E . Then, from the law of cosines,

$$u_{\text{sat}}^2 = (\tau_\oplus - u_{0,\oplus} \cos \gamma)^2 + \left(\frac{D_\perp \pi_E}{\text{AU}} + u_{0,\oplus} \sin \gamma \right)^2 - 2(\tau_\oplus - u_{0,\oplus} \cos \gamma) \left(\frac{D_\perp \pi_E}{\text{AU}} + u_{0,\oplus} \sin \gamma \right) \cos \gamma. \quad (19)$$

By measuring A at some time $A(t) = (F(t) - F_{\text{base}})/F_s$, where the F are flux measurements and F_s is the independently determined source flux, and inverting Equation (5), one can determine u_{sat}^2 and so (by inverting Equation (19)), determine π_E .

This sequence of calculations has a number of potential ambiguities, which we now discuss. First, from the ground-based light curve, only the magnitude of $u_{0,\oplus}$ is known, but not its sign. Hence, inversion of Equation (19) will yield two different answers depending on the sign chosen for u_0 . However, if τ and/or $D_\perp \pi_E/\text{AU}$ is large compared to u_0 , then the impact on the measurement of π_E will be small. This is why the method is restricted to “high-magnification events”, similarly to Gould & Yee (2012).

Applying this condition by setting $u_{0,\oplus}$ to zero, we can invert Equation (19) to obtain

$$\pi_E = \frac{\text{AU}}{D_\perp} \left(\tau_\oplus \cos \gamma \pm \sqrt{u_{\text{sat}}^2 - \tau^2 \sin^2 \gamma} \right) \quad (20)$$

From Equation (20), one can immediately see that if γ is acute, then there are two positive solutions, whereas if it is obtuse, then there is only one. (Note that π_E is positive definite because the direction of π_E is known.) This also implies that if $\pi_E \sim (\text{AU}/D_\perp) \tau_\oplus \cos \gamma$, then the error in the estimate of π_E will be large. However, both of these problems can be countered if there are additional data taken further on the decline.

At the present time, there are two values for γ that differ by $2\phi \simeq 37^\circ$. This immediately implies that Equation (20) cannot be uniquely interpreted until this ambiguity is broken by *Gaia*. In the approximation that $\sin \gamma$ is the same for both of these solutions, the difference in π_E is roughly $\Delta \pi_E \sim 0.9$, which is quite large. In principle, it is possible that the ambiguity could be resolved by the time series of *Spitzer* measurements, but this may prove difficult.

In brief, the very precise measurement of Φ_π that can be achieved either by two epochs of interferometric

imaging or one such epoch combined with a *Gaia* astrometric microlensing measurement, can enable satellite parallax measurements, even under much less favorable conditions than has heretofore been possible.

We thank the operational Paranal team led by K. Tristram and X. Hautbois. We thank Akihiko Fukui for making us aware of T. Kojima’s discovery and Szymon Kozłowski for his help.

S.D. and P.C. acknowledge Projects 11573003 supported by the National Science Foundation of China (NSFC). This work was partly supported by NSFC 11721303. This research has made use of the Jean-Marie Mariotti Center SearchCal service⁶ co-developped by LAGRANGE and IPAG, and of CDS Astronomical Databases SIMBAD and VIZIER⁷. This research has also made use of the Jean-Marie Mariotti Center Aspro2 service (Bourgès et al. 2013)⁸. Work by AG was supported by AST-1516842 from the US NSF and by JPL grant 1500811. AG received support from the European Research Council under the European Union’s Seventh Framework Programme (FP 7) ERC Grant Agreement n. [321035].

We thank the Las Cumbres Observatory and its staff for its continuing support of the ASAS-SN project. We are grateful to M. Hardesty of the OSU ASC technology group. ASAS-SN is supported by the Gordon and Betty Moore Foundation through grant GBMF5490 to the Ohio State University and NSF grant AST-1515927. Development of ASAS-SN has been supported by NSF grant AST-0908816, the Mt. Cuba Astronomical Foundation, the Center for Cosmology and AstroParticle Physics at the Ohio State University, the Chinese Academy of Sciences South America Center for Astronomy (CAS- SACA), the Villum Foundation, and George Skestos.

This paper uses data products produced by the OIR Telescope Data Center, supported by the Smithsonian Astrophysical Observatory. This work has made use of data from the European Space Agency (ESA) mission *Gaia* (<https://www.cosmos.esa.int/gaia>), processed by the *Gaia* Data Processing and Analysis Consortium (DPAC, <https://www.cosmos.esa.int/web/gaia/dpac/consortium>). Funding for the DPAC has been provided by national institutions, in particular the institutions participating in the *Gaia* Multilateral Agreement.

⁶ Available at <http://www.jmmc.fr/searchcal>

⁷ Available at <http://cdsweb.u-strasbg.fr/>

⁸ Available at <http://www.jmmc.fr/aspro2>

Software: DRS (v1.0.5; Lapeyrere et al. 2014), CANDID (Gallenne et al. 2015)

REFERENCES

- Batista, V., Beaulieu, J.-P., Bennett, D.P., et al. 2015, *ApJ*, 808, 170
- Belokurov, V. A., & Evans, N. W. 2002, *MNRAS*, 331, 649
- Bennett, D.P., Bhattacharya, A., Anderson, J., et al. 2015, *ApJ*, 808, 169
- Bourgès, L., Mella, G., Lafrasse, S., & Duvert, G. 2013, *Astrophysics Source Code Library*, ascl:1310.005
- Bramich, D. M. 2018, *A&A*, 618, A44
- Calchi Novati, S., Gould, A., Yee, J.C., et al. 2015, *ApJ*, 814, 92
- Cassan, A., & Ranc, C. 2016, *MNRAS*, 458, 2074
- Cheli, A., Duvert, G., Bourgès, L. et al. 2016, *A&A*, 589, 112
- Dalal, N., & Lane, B. F. 2003, *ApJ*, 589, 199
- Delman, F., Górski, K. M., & Richichi, A. 2001, *A&A*, 375, 701
- Dong, S., Udalski, A., Gould, A., et al. 2007, *ApJ*, 664, 862
- Einstein, A. 1936, *Science*, 84, 506
- Fukui, A., Abe, F., Ayani, K., et al. 2007, *ApJ*, 670, 423
- Gaia Collaboration, Prusti, T., de Bruijne, J. H. J., et al. 2016, *A&A*, 595, A1
- Gaia Collaboration, Brown, A. G. A., Vallenari, A., et al. 2018, *A&A*, 616, A1
- Gallenne, A., Mérand, A., Kervella, P. et al. 2015, *A&A*, 579, 68
- Gaudi, B.S., Patterson, J., Spiegel, D.S. et al. 2008, *ApJ*, 677, 1268
- Ghosh, H., DePoy, D. L., Gal-Yam, A., et al. 2004, *ApJ*, 615, 450
- Gould, A. 1992, *ApJ*, 392, 442
- Gould, A. 1994a, *ApJL*, 421, L71
- Gould, A. 2000, *ApJ*, 542, 785
- Gould, A. 2004, *ApJL*, 606, 319
- Gould, A. 2015, *JKAS*, 47, 215
- Gould, A. & Yee, J.C.. 2014, *ApJ*, 755, L17
- Gould, A. & Yee, J.C.. 2014, *ApJ*, 784, 64
- Gould, A., Miralda-Escudé, J. & Bahcall, J.N. 1994, *ApJ*, 423, L105
- GRAVITY Collaboration: Abuter, R. et al. 2017, *A&A*, 602, A94
- Hog, E., Novikov, I.D., & Polanarev, A.G. 1995, *A&A*, 294, 287
- Jayasinghe, T., Dong, S., Stanek, K. Z., et al. 2017, *The Astronomer's Telegram*, 10923
- Kochanek, C. S., Shappee, B. J., Stanek, K. Z., et al. 2017, *PASP*, 129, 104502
- Kervella, P., Thévenin, F., Di Folco, E., & Ségransan, D. 2004, *A&A*, 426, 297
- Lapeyrere, V. & Kervella, P. & Lacour, S. & et al. 2014, in *Proc. SPIE*, Vol. 9146, *Optical and Infrared Interferometry IV*, 91462D
- Lawson, P. R. 2000, *Principles of Long Baseline Stellar Interferometry*
- Hiroiyuki, M. 2017, *The Astronomer's Telegram*, 10919
- Miyamoto, M. & Yoshii, Y. 1995, *AJ*, 110, 1427
- Nucita, A. A., Licchelli, D., De Paolis, F., et al. 2018, *MNRAS*, 476, 2962
- Paczynski, B. 1986, *ApJ*, 304, 1
- Pecaut, M. J., & Mamajek, E. E. 2013, *ApJS*, 208, 9
- Rattenbury, N. J., & Mao, S. 2006, *MNRAS*, 365, 792
- Refsdal, S. 1966, *MNRAS*, 134, 315
- Sahu, K. C., Anderson, J., Casertano, S., et al. 2017, *Science*, 356, 1046
- Schlafly, E. F., & Finkbeiner, D. P. 2011, *ApJ*, 737, 103
- Shappee, B. J., Prieto, J. L., Grupe, D., et al. 2014, *ApJ*, 788, 48
- Shin, I.-G., Udalski, A., Yee, J.C. et al. 2018, *ApJ*, 863, 23
- Skrutskie, M. F., Cutri, R. M., Stiening, R., et al. 2006, *AJ*, 131, 1163
- Smith, M., Mao, S., & Paczyński, B., 2003, *MNRAS*, 339, 925
- Walker, M.A. 1995, *ApJ*, 453, 37
- Yoo, J., DePoy, D.L., Gal-Yam, A. et al. 2004, *ApJ*, 603, 139
- Zurlo, A., Gratton, R., Mesa, D., et al. 2018, *MNRAS*, 480, 236